DOI: 10.1002/ejic.201000754

High-Temperature Synthesis and Formation Mechanism of Stable, Ordered MCM-41 Silicas by Using Surfactant Cetyltrimethylammonium Tosylate as Template

Kun Zhang,*[a] Hong-Li Chen,[a] Belén Albela,[b] Jin-Gang Jiang,[a] Yi-Meng Wang,*[a] Ming-Yuan He,[a] and Laurent Bonneviot[b]

Keywords: Silicas / Mesoporous materials / Cetyltrimethylammonium tosylate / Hydrothermal synthesis / Template synthesis

Highly ordered 2D hexagonal mesostructured silicas with thick pore walls have been directly hydrothermally synthesized at high temperatures in a range from 130 to 175 °C by using the new surfactant cetyltrimethylammonium tosylate (CTATos) as template. The mesoporous structure of the synthesized MCM-41 could be maintained after heating it to reflux in boiling water for at least 24 h. The crystallization temperature, the nature of surfactants, and the relative amount of TAAOH (tetraalkylammonium hydroxide, such as TMAOH and TEAOH) to surfactant were found to be critical parameters that affect the ordering of mesophases. On the basis of the combined characterizations of X-ray diffraction (XRD), N_2 adsorption, Fourier transform infrared spectroscopy (FTIR), thermogravimetric analysis (TG), ^{13}C cross-polarization magic-angle spinning (CPMAS) solid-state NMR spectroscopy, transmission electron microscopy (TEM) and scanning electron microscopy (SEM), a new mechanism was proposed to understand the formation mechanism of highly ordered MCM-41 silicas. The enlargement of pore-wall thickness is attributed to the migration and subsequent deposition of the silicate species in the inner pore channel. This process was accelerated by the ion-exchange interaction of tetraalkylammonium cations (TAA^+) on CTA^+ cations.

Introduction

P∧P Since the birth of the M41S family of silicas with ordered and tunable mesopores, much effort has been devoted to improving the thermal, hydrothermal, and mechanical stability of these novel materials due to their potential uses in many fields such as catalysis, adsorption, support for novel metals, and also the design of hybrid materials.[1–10] MCM-41, the hexagonal phase, is undoubtedly the best known and most widely studied of this family of materials. Generally, MCM-41 silica is synthesized at mild temperatures of less than 130 °C, which usually results in imperfectly condensed mesoporous walls with a thickness of less than 1.0 nm and large amounts of terminal hydroxy groups, which makes the mesostructure unstable.[11] Direct synthesis of mesoporous silica (SBA-15) by using nonionic copolymer as template has been found the most obvious route to generate a large pore size in the range of 4.6–30.0 nm. The SBA-15 materials are claimed to be very stable because of their large wall thickness, which is around 2.0–5.0 nm.[12] However, a recent study by Galarneau et al. showed that SBA-15 mesoporous silicas are not as stable as expected in water, even at room temperature, probably due to the presence of micropores in the channels.[13] It should be mentioned that the studies on the synthesis of mesoporous silicas at high temperature mostly concentrate on SBA-15.[14–18] Very few studies focus on MCM-41 silica. Another recent development in the mesoporous community concerned the synthesis, characterization, and application of mesoporous silica membranes. The hydrothermal stability can be significantly increased through membrane thickening.[19–21] Therefore, the direct synthesis of highly ordered MCM-41 silica with thick pore walls up to 2.0 nm still attracts considerable attention.[22–29]

Recently, several studies showed that it is also possible to directly synthesize ordered mesostructured silicas by using cetyltrimethylammonium bromide (CTAB) as template at temperatures higher than 150 °C. However, it remains a real challenge to keep a good mesostructure due to the distortion of micelles or the decomposition of surfactants at such a high temperature.[27,29] Additionally, not only did different research groups obtain materials that were claimed to have different porous structures, but also the proposed mechanisms for pore-size expansion conflicted. Two mechanisms

[a] Shanghai Key Laboratory of Green Chemistry and Chemical Processes, Department of Chemistry, East China Normal University,
200062 Shanghai, China
Fax: +86-21-62232293
E-mail: kzhang@chem.ecnu.edu.cn
ymwang@chem.ecnu.edu.cn
[b] Laboratoire de Chimie, Ecole Normale Supérieure de Lyon, Institut de Chimie de Lyon, Université de Lyon,
46 Allée d'Italie, 69364 Lyon, Cedex 07, France
E-mail: Laurent.bonneviot@ens-lyon.fr

Supporting information for this article is available on the WWW under http://dx.doi.org/10.1002/ejic.201000754.

were proposed to elucidate the unit-lattice expansion of MCM-41 silica by means of high-temperature hydrothermal post-synthesis, such as the swelling action of *N*,*N*-dimethylhexadecylamine (DMHA) that decomposed from the surfactant template,[23,26] and the tetraalkylammonium-cation-inclusive mechanism.[25] It should be mentioned that, when in the presence of sodium ions, MCM-41 silicas often show poor hydrothermal and thermal stability due to the formation of deficient sites in the pore wall.[30,31] Several articles suggested that the tetraalkylammonium cations play a very important role in controlling highly ordered mesostructures. However, the exact role of tetraalkylammonium cations (TAA^+) for the unit-cell expansion was not well defined.[25,32,33]

In this report, by using the new surfactant cetyltrimethylammonium tosylate (CTATos) as template, highly ordered MCM-41 silica was synthesized through the direct hydrothermal synthesis method. When the crystallization temperature was 175 °C, the maximum pore-wall thickness was up to 2.5 nm. Even after calcination at 1123 K for 5 h and boiling in water for 24 h, the mesostructure could be maintained. The main reason for unit-lattice and pore-wall enlargement is probably due to the migration and subsequent deposition of silicate species. The silicate species are formed due to the high-temperature dissolution of disordered mesoporous silica nanoparticles. Additionally, due to the use of the new surfactant CTATos, the amount of surfactant could be significantly decreased. A high molar ratio of tetraalkylammonium hydroxide/surfactant in the mother liquor accelerates the ion exchange of TMA cations on CTA cations, which in turn speeds up the migration and deposition of silicate species in the channels.

Results and Discussion

The XRD patterns of samples synthesized at different crystallization temperatures are shown in Figure 1, when TMAOH (tetraalkylammonium hydroxide, such as TMAOH and TEAOH) was used as the base. All the samples except those synthesized at 165 °C display very similar patterns with three easily distinguished diffraction peaks, (100), (110), and (200), that feature highly ordered 2D hexagonal packing of MCM-41 silica. Moreover, with the increase in crystallization temperature from 130 to 175 °C, the d_{100} spacing of calcined samples shifted to a high value from 4.1 to 6.1 nm (Table 1), similar to the results reported by Cheng et al.,[23,24] Corma et al.,[25] Kruk et al.,[26,27] and Mokaya.[28] It is worth noting that the sample synthesized at 175 °C shows the highest intensity at the (100) diffraction peak, thereby indicating the high ordering of the obtained mesophase. Indeed, the smallest cell contraction value (1.6%; Table 1) in this sample before and after calcination also implies a well-condensed silica framework, consistent with the results characterized later by thermogravimetric analysis (TG). The TEM images of the calcined sample (Figure 2) show a hexagonal array along the [100] zone plane and a cylinder array along the [110] zone plane, thereby confirming that the calcined sample has a highly ordered 2D hexagonal mesostructure with *p6mm* symmetry, and most interestingly the pore-wall thickness is close to 3.0 nm. To the best of our knowledge, this is the first MCM-41 silica with a highly ordered structure that can be synthesized at such a high crystallization temperature (175 °C) by using cetyltrimethylammonium surfactant as template.

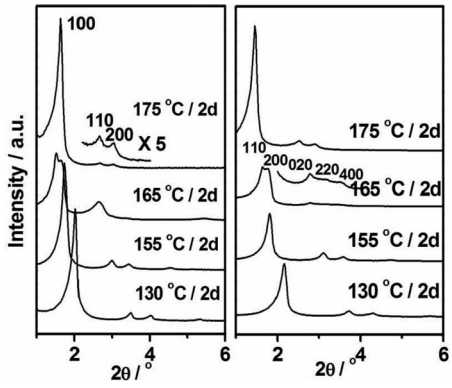

Figure 1. XRD patterns of as-prepared (left) and calcined (right) samples synthesized at varied crystallization temperatures for 2 d.

Table 1. Pore-structure data of mesoporous silicas synthesized at various crystallization temperatures.

No.	T [°C]	d_{100}[a] [nm]	d_{100}[b] [nm]	CC[c] [%]	S_{BET}[d] [$m^2 g^{-1}$]	V_{total}[e] [$cm^3 g^{-1}$]	D_{BJH}[f] [nm]	t_{BJH}[g] [nm]	D_{BdB}[h] [nm]	t_{BdB}[i] [nm]
1	130	4.4	4.1	6.8	853	0.79	2.9	1.8	3.7	1.0
2	155	5.1	4.9	3.9	953	0.97	3.6	2.1	4.4	1.3
3	165	5.8	5.4	6.9	490	0.50	3.6	2.6	4.4	1.8
4	175	6.2	6.1	1.6	487	0.53	3.6	3.4	4.5	2.5
5[j]	175	5.5	5.5	–	305	0.29	3.7	2.6	3.1	2.2
7[k]	175	5.8	5.8	–	481	0.57	3.5	3.2	4.6	2.1

[a] Value of d_{100} of as-prepared samples collected from XRD patterns. [b] Value of d_{100} of calcined samples collected from XRD patterns. [c] Cell-contraction value before and after calcination. [d] S_{BET} calculated by using the Brunauer–Emmett–Teller (BET) equation over a range of relative pressure from 0.05 to 0.3. [e] Single-point pore volume at $P/P_o = 0.99$. [f] D_{BJH} = pore size calculated with the Barrett–Joyner–Halenda (BJH) method by using the desorption branch. [g] t_{BJH}, pore-wall thickness = $2d_{100}/1.732 - D_{BJH}$. [h] D_{BdB} = pore size calculated with the Broekhoff–de Boer (BdB) method by using the desorption branch. [i] t_{BDB}, pore-wall thickness = $2d_{100}/1.732 - D_{BdB}$. [j] Sample synthesized in a CTATos/silica molar ratio of 0.045. [k] Sample synthesized by using tetraethylammonium hydroxide (TEAOH) as the base source.

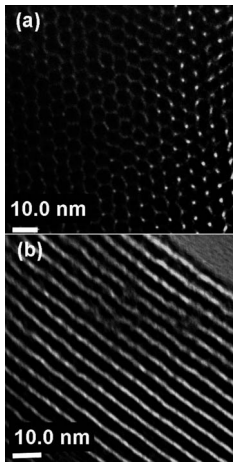

Figure 2. TEM image of calcined sample synthesized at 175 °C for 2 d: (a) along the long axis and (b) perpendicular to the long axis.

It should be mentioned that the small organic ion TMA^+ has often been used to synthesize dodecasil-3C (ZSM-39) zeolites as a structure-directing agent (SDA). To preclude the presence of dodecasil zeolites, we carried out high-angle XRD measurements (Figure S1 in the Supporting Information). The XRD patterns in the high-angle range did not show any feature peaks of dodecasil-3C (ZSM-39), thereby indicating the currently synthesized material is pure MCM-41 silica. By checking the literature, we found that the hydrothermal synthesis of dodecasil-3C zeolites was carried out at 180 °C for 10–30 d.[34,35] In our case, if the crystallization temperature was higher than 180 °C, the mesostructure collapsed, and the crystallization time was kept to 2 d. Thus, we concluded that the current materials were pure MCM-41 silicas.

As is already known, to synthesize ordered mesoporous silica with a thick silica wall, an increase in the silica/surfactant ratio is an option. We studied the influence of silica/surfactant ratio on the pore structure, especially the synthesis of MCM-41 at very low concentrations of the surfactant. The molar ratio of CTATos/silica was decreased to 0.015. Unfortunately, MCM-41 could not be formed. When the molar ratio was equal to or larger than 0.045, MCM-41 with a highly ordered structure could be synthesized at 175 °C for 2 d, as shown by XRD (Figure S2 in the Supporting Information). However, TEM observation showed that some wormlike pores had already been formed, thereby indicating a decrease in the ordering of the MCM-41 structure (Figure S3 in the Supporting Information). This means that this ratio is the critical value in the formation of highly ordered MCM-41 silicas. The textural data has been added in Table 1. Due to the decrease in the order of the structure, the pore volume and surface area decreased to 305 $m^2 g^{-1}$ and 0.29 $cm^3 g^{-1}$, respectively. It is interesting to note that even at this critical value, the pore-wall thickness can be up to 2.6 nm as calculated by the Barrett–Joyner–Halenda (BJH) method. Therefore, the current synthesis is unique.

To investigate the influence of other types of small tetraalkylammonium cations on the order of the pore structure, TEAOH as base source was also introduced into the reaction system. The sample synthesized at 175 °C for 2 d showed four XRD diffraction peaks, which indicated a highly ordered mesostructure (Figure S4 in the Supporting Information). Therefore, highly ordered MCM-41 silicas could be synthesized at a temperature of 175 °C by using CTATos as template and TMAOH or TEAOH as base.

Interestingly, a very rare 2D centered rectangular mesophase (SBA-8,[36,37] space group *cmm*) was formed at the crystallization temperature of 165 °C, thereby indicating the occurrance of mesophase transformation. So far, only two examples of the synthesis of SBA-8 (space group *cmm*) have been reported. The synthesis of SBA-8 materials is often neglected due to their intermediate nature, and sometimes they are misunderstood as a mixture of two MCM-41 mesophases. When the crystallization temperature or even calcination temperature is increased, this phase can be easily transformed into the MCM-41 mesophase. The formation mechanism is very complicated, and the discussion falls outside of this paper. However, to further substantiate that our mesophase is SBA-8, the XRD patterns at 165 °C of SBA-8 (Figure 1) were studied in more detail (Figure S5 in the Supporting Information). XRD patterns exhibited the typical characteristics of SBA-8 as synthesized previously by Stucky et al.[36] and Amoros et al.[37] The indexation of the diffraction peaks is listed in Table S1 in the Supporting Information. Calcined SBA-8 showed six well-defined diffraction peaks, thus confirming the 2D rectangular symmetry of the SBA-8 mesophase. As is well known, the centered rectangular phase consists of ovoid tubes placed on a centered rectangular lattice that is related to the *P6mm* hexagonal structure with an *a*/*b* ratio of 1.73 by a distortion along one axis. In the current synthesis, the *a*/*b* ratio derived from XRD data is 1.57, very close to the reported value 1.53.[36]

The nitrogen sorption isotherms measured at 77 K on samples synthesized at varied crystallization temperatures are shown in Figure 3. The textural properties of samples are summarized in Table 1. These adsorption–desorption isotherms are typical IV isotherms with a sharp inflection point at relative pressure 0.30–0.60 due to the capillary condensation, as shown in Figure 3 (left). This inflection is the characteristic of mesoporous materials.[38] At a low temperature of 130 °C, a sharp increase of adsorbed N_2 volume occurred for a relative pressure (P/P_0) of 0.35. This jump is irreversible: a hysteresis loop with parallel adsorption and desorption branches is observed (type H_1). The sharpness of this jump indicates the uniformity of the mesopore size. When the crystallization temperature was raised to 155 °C, the sharp reflection point shifted to a high P/P_0 value of 0.45, thereby implying an increase in the pore size. Moreover, the hysteresis loop was now found to be triangular in shape, thereby indicating the diffusion of nitrogen molecules in the channel was constrained.[39,40] The change of hysteresis shape was probably related to pore deformation, which may be ascribed to the phase transformation. If the crystallization temperature was further increased to 175 °C, the position of the reflection point was not obviously

changed, thereby indicating that the mesopore size remains almost unchanged; however, the BET surface area and total pore volume dramatically decreased to around 500 $m^2 g^{-1}$ and around 0.50 $cm^3 g^{-1}$, respectively (Table 1), probably related to the thicker pore wall with a size of 2.5 nm.[26] Note that the calcined sample synthesized at 175 °C showed an H_1 hysteresis loop, typical for SBA-15, and the pore-wall thickness up to 2.5 nm calculated by the Broekhoff–de Boer (BdB) method is very close to that of SBA-15.[12] For comparison, we also did calculations using the BJH method, and the pore-wall thickness was 3.4 nm. As far as we know, this is the largest pore-wall thickness of MCM-41 silicas.

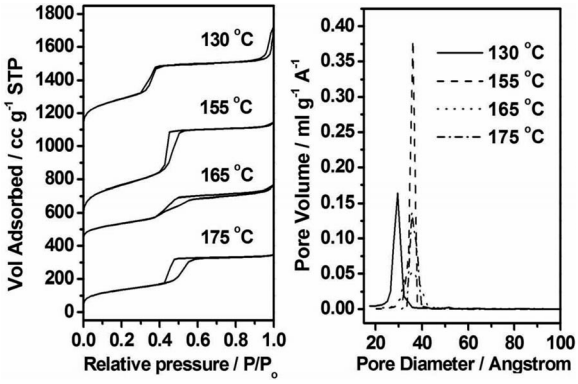

Figure 3. N_2 physisorption of samples synthesized at varied crystallization temperatures: N_2 adsorption–desorption isotherms (left) and pore-size distribution plot calculated by the BJH method from the desorption branch.

The pore-size distribution (PSD) curves calculated by the BJH method from the desorption branch are shown in Figure 3 (right). The sample synthesized at 130 °C shows a narrow pore-size distribution centered at 2.9 nm. If the crystallization temperature was further increased, the pore size was basically constant, centered at 3.6 nm, which is in contrast with the results reported by Corma et al.[25] and Kruk et al.[26,27] In those studies, the pore size of MCM-41 increased with crystallization temperature, whereas the pore-wall thickness remained constant and was always less than 1.0 nm. It should be mentioned that the calculation methods based on the Kelvin equation, in particular the BJH method, systematically underestimate pore diameters by at least 10%.[41–43] In this work, the more reliable BdB calculation method was also used to measure the pore size and wall thickness.[44,45] The pore size of two samples synthesized at 130 and 175 °C was 3.7 and 4.5 nm, respectively, much larger than those calculated by the BJH method. The wall thickness calculated by subtracting the BdB channel diameter from the unit-cell parameter increased from 1.0 to 2.5 nm when the crystallization temperature was raised from 130 and 175 °C. The thickest wall of 2.5 nm is much larger than that previously reported by Kresge et al.,[11] Corma et al.,[25] and Kruk et al.[26,27] (less than 1.0 nm), and the increase in pore-wall thickness suggests that pore size is not changed with an increase in crystallization temperature, whereas the unit cell is enlarged. Here it should be mentioned that, at high temperatures (>75 °C), the size of micelles formed by surfactants was nearly constant;[23,46] therefore it is unlikely that the unit-cell enlargement is due to the effect of temperature on the micelle size.

SEM is an effective tool to investigate the morphology evolution and formation mechanism of mesoporous silica. Figure 4 shows that all the samples are mainly made up of irregularly shaped particles of a size of several micrometers, and with an increase in temperature, the shape and size of particles was not greatly changed. SEM conservation confirmed that the extensive restructuring of MCM-41 was not done during the hydrothermal treatment, consistent with the result reported by Kruk and co-workers.[26,27] It is worth noting that, at a low crystallization temperature (<165 °C), some small silica nanoparticles of sizes less than 100 nm were observed. Interestingly, these silica nanoparticles disappeared when the hydrothermal temperature was increased, thereby implying that the high-temperature treatment accelerated the dissolution of silicate species. A close examination of TEM showed that these nanoparticles are porous silica with wormlike holes (Figure S6 in the Supporting Information).[47] As is already known, the dissolution rate of silica nanoparticles drastically depends on the size of particles, alkalinity, and reaction temperature.[13] It is important to note that, before and after crystallization, the pH of the system remained constant, close to 11.5. At higher crystallization temperatures and higher alkalinity, the smaller silica nanoparticles can be easily decomposed to the silicate species, such as monomer or oligomer. By responding to that with an increase in crystallization temperature, these nanoparticles gradually disappeared. The formed silicate species could migrate and deposit into the inner channel of MCM-41 silica, and therefore the pore-wall thickness was strengthened.

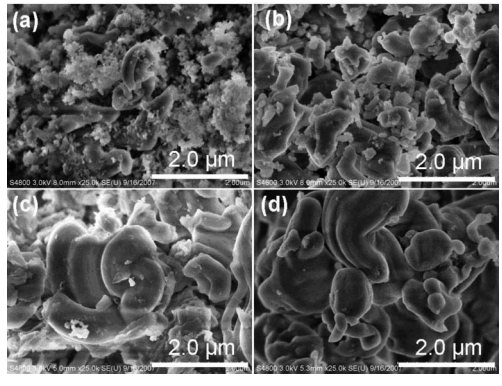

Figure 4. SEM images of samples synthesized at varied crystallization temperatures: (a) 135, (b) 155, (c) 165, and (d) 175 °C; snowlike amorphous silicas are significantly decreased with an increase in crystallization temperature.

Thermogravimetric analysis (TG) curves of the as-synthesized silica synthesized at varied crystallization temperatures are shown in Figure 5. All the samples show a mass loss below 120 °C due to desorption of physisorbed water. Interestingly, the mass loss at this stage decreases with an

increase in crystallization temperature, which could be attributed to better condensation of silica walls at high temperature and more hydrophobicity. The second mass loss in the 130–450 °C range is assigned to the decomposition of organic species including surfactant and TMA cations. Due to the overlap of the two peaks representing the decomposition temperature, it is difficult to define the molar ratio of CTA^+/TMA^+. The samples show a further mass loss between 500 and 700 °C, which we ascribe to dehydroxylation of the silicate frameworks. This mass loss is the lowest for the sample synthesized at 175 °C, which is an indication of the higher degree of polymerization of the silicate frameworks.

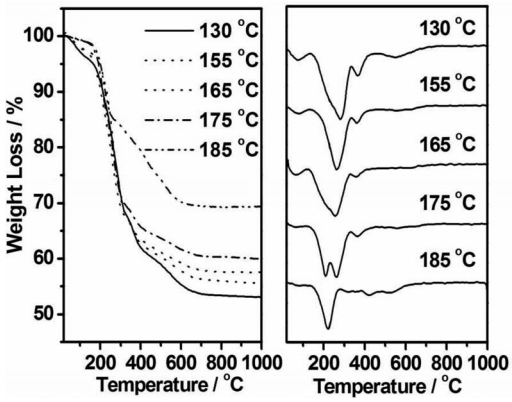

Figure 5. TG-DTG curve of as-prepared mesoporous silicas synthesized at various crystallization temperatures.

It is well known that a higher condensation degree of the silica-based inorganic framework can significantly improve the hydrothermal, thermal, and mechanical stability of mesoporous silicas.[48] However, the increased thickness of the pore wall with an increase in reaction temperature cannot be explained merely by high condensation of silicate, as continued wall building requires additional silicate species that must be transported into the channel from the mother liquor. Additionally, the differential thermogravimetric (DTG) curve shows interesting information on the decomposition of the surfactant template. With an increase in crystallization temperature, the weight-loss peak at around 280 °C is split into two peaks, thereby indicating that the surfactants are decomposed into two species. If the temperature is further increased to 185 °C, only one weight-loss peak centered at 223 °C is observed. It should be mentioned that, at this temperature, the mesostructure of this material is partially collapsed, probably due to the complete decomposition of surfactant template.

In fact, the balance of silica mass in the system can offer further evidence of the migration–redeposition of silicate species in the inner channel. The yield of each synthesis and the data on the balance of silica mass derived from TG analysis is listed in Table 2. The yield of samples synthesized at a higher reaction temperature remains constant, thus indicating that the silica mass is balanced. The way to check the silica mass based on the yield of the final product is not completely precise due to the loss in the solid collection, especially if the sample synthesized at lower reaction temperatures than 130 °C has a large quantity of nanoparticles of a size of less than 100 nm, as observed by the SEM images in Figure 4. During filtration, these nanoparticles can pass easily through the filter. Therefore, the yield of this sample is a rough estimate. The more precise and better way to check the silica mass balance is on the basis of the results of thermogravimetric analysis in Figure 5. With an increase in reaction temperature, the molar ratio of surfactant/silica is decreased from 0.143 to 0.088, thus implying that the percentage of silica in the solid is raised. The increase of residual mass from 53.0 to 69.6 further confirms this point. Based on the TG-DTG analysis, we confirmed that the silicate species can transport into the channel and subsequent deposition leads to the pore-wall thickening, which is consistent with the results of SEM observation and N_2 physisorption.

Table 2. Yield of each sample synthesized at various crystallization temperatures for 2 d.

No.	T [°C]	Yield[a] [g]	Surfactant/silica[b] (molar ratio)	RM[c] [%]
1	130	8.7	0.143	53.0
2	155	12.1	0.131	55.6
3	165	11.8	0.125	57.5
4	175	11.8	0.121	60.0
5	185	12.0	0.088	69.6

[a] Collected after filtration and drying at 80 °C. [b] Calculated on the basis of thermogravimetric analysis (TG). [c] RM means residual mass in units of percentage obtained form the TG analysis at 1273 K.

The FTIR spectra of as-prepared MCM-41 silicas synthesized at different crystallization temperatures are shown in Figure 6. The lowest frequency mode (460 cm^{-1}) is used for intensity calibration. The 500–650 cm^{-1} region provides information on specific silicate rings typical of the zeolitic structure. For a sample synthesized at 130 °C, one peak at 564 cm^{-1} is observed, which is assigned to the vibration of

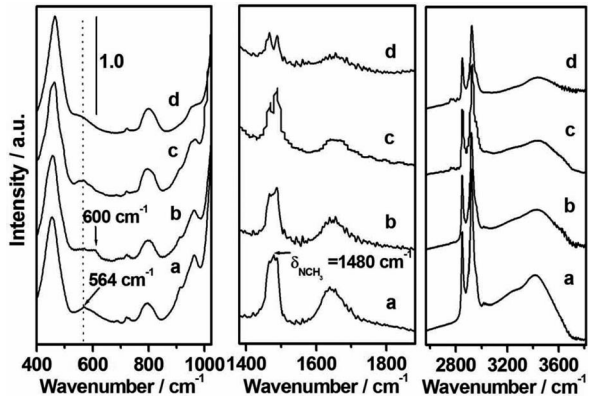

Figure 6. FTIR spectra of as-prepared MCM-41 silicas synthesized at (a) 130, (b) 165, (c) 175, and (d) 185 °C for 2 d.

cyclic siloxane within the inorganic framework.[49,50] As far as we know, this is the first example that MCM-41 silica exhibits atomic ordering in the pore wall when using solo surfactant CTA^+ as template. Similar results have been reported for the "so-called molecularly ordered" silicate lamellar materials.[51,52] When the crystallization temperature was increased to 165 °C, another vibration band can be detected around 600 cm^{-1}, and there is good agreement in the literature to attribute this broad band, generally observed in sol–gel silica materials, to residual cyclic structures present in the silica network.[49–52]

Most interestingly, when the crystallization temperature was increased to 175 °C, this new band centered at 600 cm^{-1} disappears. After further increasing the crystallization temperature to 185 °C, all the bands attributed to the cyclic siloxane vibrations disappeared, thus indicating low stability of cyclic siloxanes. In short, the structural evolution of the silica walls with crystallization temperature evidences the dissolution and restructuring of silicate species in the confined channel during hydrothermal treatment. It is possible that the redeposition of the silicate species strengthens the pore-wall thickness and leads to the expansion of the unit cell of currently synthesized mesoporous silicas. Similar atomic ordering with the inorganic framework, when TEAOH was incorporated into the synthetic system, is also observed (Figure S1 in the Supporting Information).

The evolution of organic species in the materials was also monitored by FTIR. The absorption bands at 2958 and 2870 cm^{-1} are assigned to symmetric and asymmetric CH_2 stretching modes, ν_s and ν_{as}, in long C_{16} hydrocarbon chains of CTA^+ cations.[9] With an increase in crystallization temperature, the intensity of these two bands decreased by 23.7 and 50.0% at 165 and 185 °C, respectively, thereby indicating that some CTA^+ ions are thermally decomposed and subsequently removed from the channels. It is worth noting that, as the crystallization temperature increased, the intensity of the absorption band at 1480 cm^{-1} assigned to the N–CH_3 vibration from the hydrophilic head of the surfactant molecules gradually decreased, thereby implying that the surfactant is decomposed to electrically neutral $C_{16}H_{33}(CH_3)_2N$ molecules (*N*,*N*-dimethylhexadecylamine, DMHA). A similar decomposition mechanism of surfactant was proposed by Cheng et al.[23,24] and Sayari et al.,[26,27] and these authors suggested that pore size and unit-lattice enlargement were attributed to the swelling action of decomposed species from surfactant molecules.[23,26,27,53] The elemental analysis data of as-synthesized samples indicates that the carbon/nitrogen molar ratio (denoted as C/N) decreased as the unit-cell expansion proceeded (Table S2 in the Supporting Information). For example, C/N is 15 for MCM-41 prepared at 130 °C for 2 d; for MCM-41 synthesized at 175 °C for 2 d, it is 14. The observed variation of C/N during hydrothermal treatment can be partially related to decomposition of CTA^+ (C/N = 19) to DMHA (C/N = 18). However, as the C/N decrease is larger than that expected (C/N = 18), one can expect that TMA^+ is incorporated into the micelles during the hydrothermal treatment similarly to the high-temperature synthesis done by Corma et al.[25] They pointed out that the swelling of mesoporous materials is always accompanied by a gradual increase in the content of TAA^+ cations, but with constant pore-wall thickness (ca. 1.0 nm). It should be mentioned that in our system, the molar ratio of TMA^+/CTA^+ was close to 4.0, much larger than 2.3 reported by Corma and co-workers.[25] It is possible that a higher molar ratio of TMA^+/CTA^+ accelerates the ion-exchange rate of TMA^+ on CTA^+ cations.

The ^1H-^{13}C cross-polarization (CP) magic angle spinning (MAS) NMR spectra (Figure S2 in the Supporting Information) reveal that some surfactant $C_{16}H_{33}(CH_3)_3N^+$ cations decompose to form electrically neutral $C_{16}H_{33}(CH_3)_2N$ molecules in MCM-41 silicas prepared at 165 °C for 48 h. The presence of two peaks at around δ = 46 and around 60 ppm is indicative of the formation of DMHA,[53] consistent with the results of FTIR. It was found that the decomposition mechanism is not dependent on the synthetic system; the crystallization temperature is the most critical reaction factor. It should be mentioned that when CTAB (counteranion = Br^-) was used as a template, at high temperature a mixture phase of MCM-41 and MCM-50 was found. More importantly, in our system an additional peak centered at δ = 57 ppm can be observed, which is assigned to free rotating TMA^+ cations, consistent with the results of elemental analysis. To prove the ion-exchange interaction of TMA^+ cations on the CTA^+ cation in the mesoporous channel, we designed a blank experiment. TMABr was mixed with as-preapred MCM-41 with surfactants in 95% ethanol solution, and we found that even the molar ratio of TMA^+/CTA^+ was 2.5. After one exchange, half of the surfactant in the channel was exchanged. After three exchanges, all the surfactant in the channel was replaced by TMA^+ cations (Figure S7, sample a). This further confirmed that TMA^+ involves the unit-lattice expansion process during high-temperature hydrothermal treatment.

The stability of MCM-41 silica synthesized at 175 °C for 2 d was evaluated by heating it to reflux in boiling water and high-temperature calcination. The XRD patterns showed that even when the sample was heated to reflux at 100 °C for 24 h or calcined at 850 °C for 5 h, the mesostructure of MCM-41 silica could be maintained (Figure S8 in the Supporting Information), thereby indicating that this material has a strong thermal and hydrothermal stability. Obviously, the high stability of our materials is attributed to the pore-wall thickening.

Indeed, Kruk et al. first proposed the formation mechanism of pore-size expansion of MCM-41 silica by means of hydrothermal treatment, in which in situ generation of DMHA acts as an expander and is primarily responsible for the formation of larger-pore materials.[26,27,53] Obviously, in our case, even though a large quantity of DMHA, decomposed from surfactant template, is produced at higher crystallization temperature, the pore size remains constant. Thus, Kruk's mechanism cannot fully interpret the high-temperature unit-lattice expansion process. Moreover, Corma et al. proposed that the unit-lattice expansion is related to the incorporation of the TMA^+ cation into the

channel.[25] However, the reasons for TMA^+ incorporation and the exact role of TMA^+ cations in the unit-cell enlargement are not clearly elucidated. Based on the current investigation, a new mechanism of the unit-cell enlargement is proposed to elucidate the structural evolution of MCM-41 silicas with increasing crystallization temperature and to understand the role of tetraalkylammonium cations in the unit-lattice expansion of MCM-41 silicas in Scheme 1.

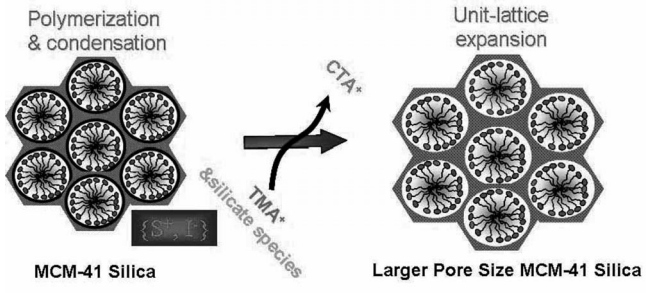

Scheme 1. Proposed mechanism for the formation of highly ordered 2D hexagonal MCM-41 silica with thick pore walls.

It should be mentioned that in the literature cationic surfactant CTAB is often used on a large scale to synthesize highly ordered MCM-41 silica. In the current synthesis of MCM-41 silica, the surfactant cetyltrimethylammonium tosylate (CTATos) is used. The only difference is that the counteranion Br^- in the CTAB surfactant is replaced by tosylate in CTATos (see the Supporting Information for the formula structure). The introduction of tosylate as the surfactant counteranion can significantly decrease the use of surfactant in the synthesis. Thus, if the concentration of TAAOH is constant, the molar ratio of TAA^+/CTA^+ is greatly increased. For example, if the molar ratio of CTATos/silica is 0.045, in the current synthesis, the molar ratio of TAA^+/CTA^+ is up to 7.8. The higher molar ratio of TAA^+/CTA^+ can significantly accelerate the ion-exchange interaction of TMA^+ cations on the CTA^+ cations, which in turn speeds up the migration and deposition of silicate species in the channels of MCM-41 silica.

But what is the origin of silicate species? Continued wall building in MCM-41 silica with constant pore size needs additional silicate species, which must be transported into the channel from the mother liquor. SEM images show that with increasing crystallization temperature, the disordered mesoporous silica nanoparticles gradually disappeared, and finally only pure MCM-41 silica nanoparticles were found. Clearly, the higher temperature and basicity accelerated the dissolution of disordered mesoporous silica nanoparticles, and new silicate species as building units of pore walls were formed. Therefore, the enlargement of the pore-wall thickness and unit lattice are attributed to the migration and subsequent deposition of silicate species, which are decomposed from the dissolution of disordered mesoporous silica nanoparticles.

Conclusion

The formation mechanism of MCM-41 silicas with high stability has been presented. The enlargement of the unit lattice and pore-wall thickness is attributed to the migration and deposition of silicate species, which come from the dissolution of disordered porous silica nanoparticles at high crystallization temperature and high alkalinity of the reaction system. The high molar ratio of TAA^+/CTA^+ accelerates the ion-exchange interaction of TAA^+ cations on the surfactant CTA^+ cations, which in turn speeds up the migration and deposition of silicate species in the channels of MCM-41 silicas. Therefore, high-quality MCM-41 silicas have been synthesized at high temperature by using the new surfactant cetyltrimethylammonium tosylate as template, and the resulting materials show high thermal and hydrothermal stability. Efforts are underway to take advantage of this better understanding of the synthetic procedure to design mesoporous zeolites with hierarchical porosity.

Experimental Section

Synthesis of MCM-41: All reagents used were purchased from Sigma–Aldrich except cetyltrimethylammonium tosylate, which was from Merck. In a typical synthesis procedure, cetyltrimethylammonium tosylate (CTATos; 7.40 g; molecular structure in the Supporting Information) was dissolved in water (120 mL), and the mixture was stirred at 60 °C for 1 h. An aqueous solution of tetramethylammonium hydroxide (TMAOH; 63mL, 1.0 M) was added to water (107 mL), followed by the addition of fumed silica (10.78 g) under vigorous agitation. After stirring at 60 °C for 1 h, the silicate solution was added dropwise into the CTATos solution. The molar ratio for the collected gel composition is $1SiO_2$:0.09CTATos:0.35TMAOH:$79.9H_2O$. The mixture was stirred continually at 60 °C for 2 h and then loaded into a 250 mL Teflon-lined steel autoclave, in which the gel mixture was pre-aged at 35 °C for 48 h, then heated at 175 °C for 48 h. It is important to note that the molar ratio of TMA^+/CTA^+ in the current gel composition is close to 4.0, which is much larger than that reported in the literature.[23–27] The final products were collected by filtration, washed, and dried. To remove the templates, the products were finally heated at reflux under air at 550 °C for 6 h. Note that when TEAOH was used as base source, highly ordered MCM-41 silicas at high crystallization temperatures could also be synthesized.

Hydrothermal Stability Test: Calcined MCM-41 (0.1 g) was boiled for different periods of time in distilled water (50 mL) by using a flask equipped with a reflux condenser. XRD patterns were obtained after this boiled sample was subsequently filtered and dried in an oven at 373 K. According to XRD analysis, loss in the XRD intensity relative to that of the same sample before the boiling treatment was used to judge the hydrothermal stability.

Physical Measurements: X-ray diffraction (XRD) patterns were collected with a Bruker D8 AVANCE instrument by using Cu-K_α radiation (λ = 1.5418 Å) at 40 kV and 40 mA. Nitrogen adsorption–desorption isotherms were recorded at 77 K with a Quantachrome Autosorb-3B instrument after activating the sample under vacuum at 473 K for at least 10 h. The specific surface areas were evaluated by using the BET method, and the total pore volume was determined from the amount adsorbed at a relative pressure of about

0.98. The pore-size distribution curves were calculated from the analysis of the desorption branch of the isotherms by using the BdB algorithm. FTIR spectra were recorded with a Nicolet Fourier transform infrared spectrometer (NEXUS 670) using the KBr technique. SEM images were taken with a Hitachi S-4800 microscope. TEM analysis was performed with a JEOL 2010F microscope equipped with a field-emission gun and operated at 200 kV. Thermogravimetric analysis (TG) was performed with a Perkin–Elmer TGA analyzer at a heating rate of 10 °C min^{-1} under an airflow. Elemental analyses of CHNS were carried out with a Perkin–Elmer 2400 series II CHNS/O analyzer. The solid ^{13}C CPMAS NMR spectroscopic measurements were collected with a Bruker DSXv400 spectrometer [cross polarization (CP) was used for both], and at 100.6 MHz a 6 μs ($h = p/2$) pulse was used with a repetition time of 3 s. The spinning rate of the rotor was about 5 kHz, and the number of scans was 10000.

Supporting Information (see footnote on the first page of this article): Surfactant molecular structure, XRD patterns, TEM images, FTIR spectra, ^{1}H-^{13}C CP MAS NMR spectra and elemental analysis data of related samples, and indexation of the XRD patterns of mesoporous SBA-8.

Acknowledgments

This work is supported by the National Natural Science Foundation of China (project 21003050 and key project 20890122) and the Shanghai Municipal Natural Science Foundation (project 10ZR1410500). K. Z. acknowledges the French Ministry of Education and Rhône-Alps (MIRA 2006) for his doctoral fellowship. Martine Simon is also warmly acknowledged for her technical support in IR spectroscopy measurements. We thank the referees for their constructive comments.

[1] A. Corma, *Chem. Rev.* **1997**, *97*, 2373–2419.
[2] A. Taguchi, F. Schüeth, *Microporous Mesoporous Mater.* **2005**, *77*, 1–45.
[3] J. Liu, Y. S. Shin, Z. M. Nie, J. H. Chang, L. Q. Wang, G. E. Fryxell, W. D. Samuels, G. J. Exarhos, *J. Phys. Chem. A* **2000**, *104*, 8328–8339.
[4] V. Dufaud, F. Beauchesne, L. Bonneviot, *Angew. Chem. Int. Ed.* **2005**, *44*, 3475–3477.
[5] S. Abry, B. Albela, L. Bonneviot, *C. R. Chim.* **2005**, *8*, 741–752.
[6] A. Badiei, L. Bonneviot, N. Crowther, G. M. Ziarani, *J. Organomet. Chem.* **2006**, *691*, 5911–5919.
[7] S. Calmettes, B. Albela, O. Hamelin, S. Ménage, F. Miomandre, L. Bonneviot, *New J. Chem.* **2008**, *32*, 727–737.
[8] S. Abry, A. Thibon, B. Albela, P. Delichère, F. Banse, L. Bonneviot, *New J. Chem.* **2009**, *33*, 484–496.
[9] K. Zhang, B. Albela, M. Y. He, Y. M. Wang, L. Bonneviot, *Phys. Chem. Chem. Phys.* **2009**, *11*, 2912–2921.
[10] S. Abry, F. Lux, B. Albela, A. Artigas-Miquel, S. Nicolas, B. Jarry, P. Perriat, G. Lemercier, L. Bonneviot, *Chem. Mater.* **2009**, *21*, 2349–2359.
[11] C. T. Kresge, M. E. Leonowicz, W. J. Roth, J. C. Vartuli, J. S. Beck, *Nature* **1992**, *359*, 710–712.
[12] D. Zhao, J. Feng, Q. Huo, N. Melosh, G. H. Fredrickson, B. F. Chmelka, G. D. Stucky, *Science* **1998**, *279*, 548–552.
[13] A. Galarneau, M. Nader, F. Guenneau, F. Di Renzo, A. Gedeon, *J. Phys. Chem. C* **2007**, *111*, 8268–8277.
[14] A. Vinu, V. Murugesan, W. Böhlmann, M. Hartmann, *J. Phys. Chem. B* **2004**, *108*, 11496–11505.
[15] M. Hartmann, A. Vinu, *Langmuir* **2002**, *18*, 8010–8016.
[16] Y. Han, D. Li, L. Zhao, J. Song, N. Li, Y. Di, C. Li, S. Wu, X. Xu, X. Meng, K. Lin, F. S. Xiao, *Angew. Chem. Int. Ed.* **2003**, *42*, 3633–3637.
[17] D. Li, Y. Han, J. Song, L. Zhao, X. Xu, Y. Di, F. S. Xiao, *Chem. Eur. J.* **2004**, *10*, 5911–5922.
[18] E. B. Celer, M. Jaroniec, *J. Am. Chem. Soc.* **2006**, *128*, 14408–14414.
[19] P. Kumar, V. V. Guliants, *Microporous Mesoporous Mater.* **2010**, *132*, 1–14.
[20] H. L. Castricum, A. Sah, R. Kreiter, D. H. A. Blank, J. F. Vente, J. E. ten Elshof, *J. Mater. Chem.* **2008**, *18*, 2150–2158.
[21] L. Huang, S. Kawi, K. Hidajat, S. C. Ng, *Microporous Mesoporous Mater.* **2005**, *82*, 87–97.
[22] D. Khushalani, A. Kuperman, G. A. Ozin, K. Tanaka, J. Garces, M. M. Olken, N. Coombs, *Adv. Mater.* **1995**, *7*, 842–847.
[23] C. F. Cheng, W. Zhou, J. Klinowski, *Chem. Phys. Lett.* **1996**, *263*, 247–252.
[24] C. F. Cheng, W. Zhou, D. H. Park, J. Klinowski, M. Hargreaves, L. F. Gladden, *J. Chem. Soc. Faraday Trans.* **1997**, *93*, 359–363.
[25] A. Corma, Q. Kan, M. T. Navarro, J. Perez-Pariente, F. Rey, *Chem. Mater.* **1997**, *9*, 2123–2126.
[26] M. Kruk, M. Jaroniec, A. Sayari, *J. Phys. Chem. B* **1999**, *103*, 4590–4598.
[27] M. Kruk, M. Jaroniec, A. Sayari, *Microporous Mesoporous Mater.* **1999**, *27*, 217–229.
[28] R. Mokaya, *Chem. Commun.* **2001**, 1092–1093.
[29] N. Xiao, L. Wang, S. Liu, Y. C. Zou, C. Y. Wang, Y. Y. Ji, J. W. Song, F. Li, X. Meng, F. S. Xiao, *J. Mater. Chem.* **2009**, *19*, 661–665.
[30] R. Ryoo, J. M. Kim, C. H. Ko, C. H. Shin, *J. Phys. Chem.* **1996**, *100*, 17718–17721.
[31] C. H. Ko, R. Ryoo, *Chem. Commun.* **1996**, 2467–2468.
[32] A. Badiei, S. Cantournet, M. Morin, L. Bonneviot, *Langmuir* **1998**, *14*, 7087–7090.
[33] B. Echchahed, M. Morin, S. Blais, A. Badiei, G. Bergault, L. Bonneviot, *Microporous Mesoporous Mater.* **2001**, *44–45*, 53–63.
[34] J. J. Seral, S. Uriel, J. Coronas, *Eur. J. Inorg. Chem.* **2008**, *31*, 4915–4919.
[35] S. J. Weigel, J. C. Gabriel, E. G. Puebla, A. M. Bravo, N. J. Henson, L. M. Bull, A. K. Cheetham, *J. Am. Chem. Soc.* **1996**, *118*, 2427–2435.
[36] D. Y. Zhao, Q. S. Huo, J. L. Feng, J. M. Kim, Y. J. Han, G. D. Stucky, *Chem. Mater.* **1999**, *11*, 2668–2672.
[37] J. El Haskouri, S. Cabrera, M. Caldes, C. Guillem, J. Latorre, A. Beltran, D. Beltran, M. D. Marcos, P. Amoros, *Chem. Mater.* **2002**, *14*, 2637–2643.
[38] K. S. W. Sing, D. H. Everett, R. A. W. Haul, L. Moscow, R. A. Pierotti, J. Rouquérol, T. Siemieniewska, *Pure Appl. Chem.* **1985**, *57*, 603–619.
[39] M. Kruk, M. Jaroniec, A. Sayari, *Langmuir* **1997**, *13*, 6267–6273.
[40] B. L. Newalkar, S. Komarneni, *Chem. Mater.* **2001**, *13*, 4573–4579.
[41] E. P. Barrett, L. G. Joyner, P. P. Halenda, *J. Am. Chem. Soc.* **1951**, *73*, 373–379.
[42] M. Kruk, M. Jaroniec, A. Sayari, *Chem. Mater.* **1999**, *11*, 492–500.
[43] Z. Luan, E. M. Maes, P. W. Van Der Heide, D. Zhao, R. S. Czernuszewicz, L. Kevan, *Chem. Mater.* **1999**, *11*, 3680–3686.
[44] J. C. P. Broekhoff, J. H. de Boer, *J. Catal.* **1967**, *9*, 8–14.
[45] W. W. Lukens Jr., P. Schmidt-Winkel, D. Zhao, J. Feng, G. D. Stucky, *Langmuir* **1999**, *15*, 5403–5409.
[46] N. A. Mazer, G. B. Benedek, M. C. Carey, *J. Phys. Chem.* **1976**, *80*, 1075–1085.
[47] C. Urata, Y. Aoyama, A. Tonegawa, Y. Yamauchi, K. Kuroda, *Chem. Commun.* **2009**, 5094.
[48] T. Mori, Y. Kuroda, Y. Yoshikawa, M. Nagao, S. Kittaka, *Langmuir* **2002**, *18*, 1595–1603.

[49] H. Y. Fan, C. Hartshorn, T. Buchheit, D. Tallant, R. Assink, R. Simpson, D. J. Kissel, D. J. Lacks, S. Torquato, C. J. Brinker, *Nat. Mater.* **2007**, *6*, 418–423.
[50] P. Innocenzi, P. Falcaro, *J. Phys. Chem. B* **2003**, *107*, 4711–4717.
[51] S. C. Christiansen, D. Zhao, M. T. Janicke, C. C. Landry, G. D. Stucky, B. F. Chmelka, *J. Am. Chem. Soc.* **2001**, *123*, 4519–4529.
[52] K. Zhang, Y. M. Wang, B. Albela, L. Chen, M. Y. He, L. Bonneviot, *New J. Chem.* **2009**, *33*, 2479–2485.
[53] A. Sayari, M. Kruk, M. Jaroniec, I. L. Moudrakovski, *Adv. Mater.* **1998**, *10*, 1376–1379.

Received: July 10, 2010
Published Online: November 18, 2010

